Article

A Novel Dual-Rotor Ultrasonic Motor for Underwater Propulsion

Xiaolong Lu [1,*], **Zhiwen Wang** [1], **Hui Shen** [1], **Kangdong Zhao** [1], **Tianyue Pan** [1], **Dexu Kong** [1] **and Jens Twiefel** [2]

1   State Key Lab of Mechanics and Control of Mechanical Structures, Nanjing University of Aeronautics & Astronautics, Nanjing 210016, China; wangzhiwen@nuaa.edu.cn (Z.W.); shenhui115@nuaa.edu.cn (H.S.); zhaokangdong@nuaa.edu.cn (K.Z.); pty11235@nuaa.edu.cn (T.P.); kdx@nuaa.edu.cn (D.K.)
2   Institute of Dynamics and Vibration Research, Leibniz University Hannover, Appelstraße 11, 30167 Hannover, Germany; twiefel@ids.uni-hannover.de
*   Correspondence: long_8446110@nuaa.edu.cn; Tel.: +86-25-84896346

check for updates

Abstract: Micro underwater vehicles (MUVs) have been highlighted recently for underwater explorations because of their high maneuverability, low price, great flexibility, etc. The thrusters of most conventional MUVs are driven by electromagnetic motors, which need big mechanical transmission parts and are prone to being interrupted by the variance of ambient electromagnetic fields. In this paper, a novel dual-rotor ultrasonic motor with double output shafts, compact size, and no electromagnetic interference is presented, characterized, and applied for actuating underwater robots. This motor was composed of a spindle-shaped stator, pre-pressure modulation unit, and dual rotors, which can output two simultaneous rotations to increase the propulsion force of the MUV. The pre-pressure modulation unit utilized a torsion spring to adjust the preload at the contact faces between the stator and rotor. The working principle of the ultrasonic motor was developed and the vibration mode of the stator was analyzed by the finite element method. Experimental results show that the no-load rotary speed and stalling torque of the prototype ultrasonic motor were 110 r/min and 3 mN·m, respectively, with 150 V peak-to-peak driving voltage at resonance. One underwater robot model equipped with the proposed ultrasonic motor-powered thruster could move at 33 mm/s immersed in water. The dual-rotor ultrasonic motor proposed here provides another alternative for driving MUVs and is appropriate for developing specific MUVs when the electromagnetic interference issue needs to be considered.

Keywords: piezoelectric actuator; underwater robot; propeller; torsional spring; dual-rotor

1. Introduction

Underwater vehicles have developed rapidly in the last two decades and intelligent micro underwater vehicles (MUVs) have been emerging as an effective platform for scientists and engineers to explore oceans for environmental monitoring, animal protection, resources exploration, etc. [1,2]. Concerning the propulsion force of MUVs, electromagnetic motors integrated with big mechanical transmission parts are normally selected to power the propellers. Furthermore, twin propeller engines were developed to increase the power of MUVs [3,4]. However, utilizing electromagnetic motors to drive pairs of propellers increases the complexity and occupies more inside space of MUVs [5–8], affecting its reliability concerning intensive electromagnetic interference, and limiting its versatility with less functional units [9–11]. Therefore, current MUVs still face the compromise between functionality and size miniaturization [12].
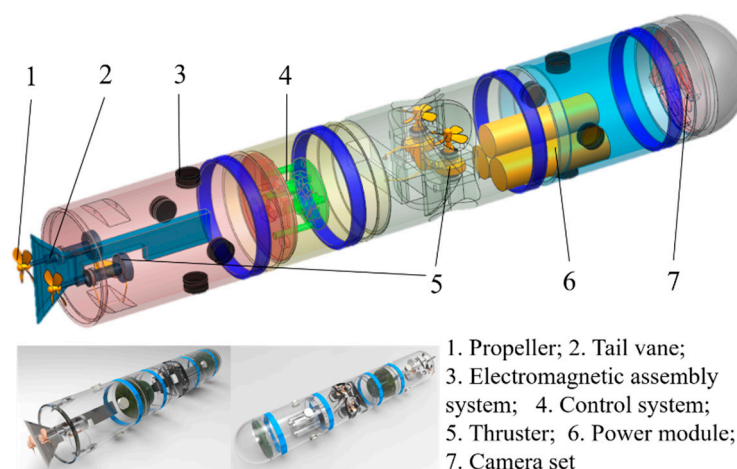
Ultrasonic motors excited by piezoelectric materials can vibrate at ultrasound frequency and output mechanical forces via the contact friction between the stator and rotor [13–15]. Compared to electromagnetic motors, ultrasonic motors have the advantages of no electromagnetic interference, low noise, high torque to mass ratio and compact structure, as well as showing great potential for optical engineering, biomedical instruments and auto robots, etc. [16]. Wang et al. proposed a high-speed rotary ultrasonic motor and discussed its capability for driving micro air vehicles [17–19]. Hunstig summarized the features of piezoelectric motors and discussed their applications and prospective [20]. Liu et al. proposed a piezoelectric actuator using different bending vibration modes to perform linear or rotary motions [21–23]. Most recently, Lu et al. demonstrated a disk-type inertial rotary motor with a no-load speed of 2200 r/min and stalling torque of 0.5 mN·m, which can be used for building a single shaft-type thruster to actuate a spherical underwater robot model moving at different operation patterns [24]. Considering the electromagnetic interference and size limitation, ultrasonic motors are competitive to traditional electromagnetic motors. This research gives basic guidance for developing novel thrusters powered by ultrasonic motors.

In this paper, a new type of dual-rotor ultrasonic motor for underwater propulsion was designed, analyzed, manufactured, and tested. By means of torsion spring adjustment, the pre-pressure between the driving foot of the stator and the outer surface of the rotors were modulated, and the rotors, fixed at parallel shafts, were driven to rotate reversely and simultaneously via the contact friction when the stator vibrated at longitudinal mode. Based on the numerical simulation; critical size parameters and the working mode of the stator were determined. The vibration performance of the stator was measured and the mechanical characteristics of the prototype motor were tested. Finally, one pair of propellers were mounted to the shaft ends of the prototype motor to build a thruster for testing the propulsion behavior with an underwater robot model.
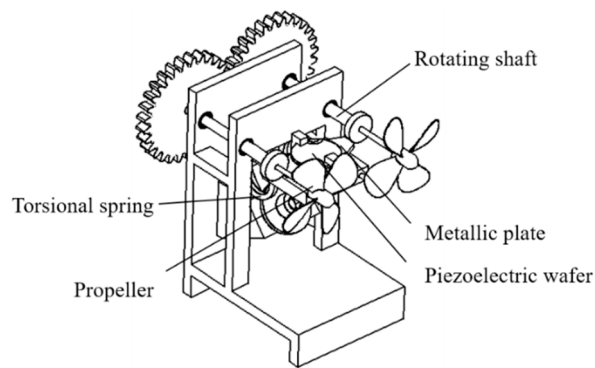
2. Structure Design

2.1. Configuration of the Motor

Figure 1 displays the three-dimensional model of an underwater robot actuated by ultrasonic motors, which can output efficient propulsion through one pair of propellers assembled to the parallel shaft ends. Figure 2 shows detailed structures of the dual-rotor ultrasonic motor employed for underwater propulsion. This motor was mainly composed of a pre-pressure modulating unit, a stator, a gear unit, two rotors, and a bracket.

1. Propeller; 2. Tail vane;
3. Electromagnetic assembly system; 4. Control system;
5. Thruster; 6. Power module;
7. Camera set

Figure 1. Three-dimensional model of the underwater robot.

Figure 2. Configuration of the ultrasonic motor.

The pre-pressure modulating unit included a torsion spring and a supporting slider. The torsion spring fixed to the stator's side served as the clamping for the stator, while also adjusting the preload on the contact faces between the stator and rotors by its torsional deformation. The stator unit comprised of a spindle-shaped metal plate and a round circular piezoelectric ceramic wafer. The piezoelectric wafer was bonded to the top face of the metal plate with epoxy resin, with its polarization direction perpendicular to the metal plate. Two ends of the stator were used as driving feet, which had an oblique angle at the upper edge in order to increase the contact area between the stator and rotor [25]. The gear unit consisting of a pair of gears engaged with each other was fixed to the rotary shafts, respectively, ensuring the same rotation speed and opposite steering of shafts rotation at both ends. The gear unit guaranteed the same thrust for propellers at both ends and thus prevented the micro-underwater robot from unexpected turning. The rotor unit comprised of two driving disks assembled at two parallel rotary shafts and two pairs of bearings were adopted to support the shaft rotation. In particular, thin-type deep groove ball bearings (inner diameter: 4 mm; outer diameter: 7 mm; thickness: 2.5 mm) were selected and integrated into the walls of the bracket. Based on this dual-rotor design, one pair of propellers with opposite turning directions could be installed to each shaft end and output propulsion for the underwater robot.

2.2. Pre-Pressure Modulation Method

Figure 3 illustrates the pre-pressure modulating unit of the ultrasonic motor. It can be seen that the torsion spring was mounted to the tilted side of the supporting slider, with another end installed with a base for holding the stator. The opening structure of the clamping ends on top of the base could minimize the clamping effect to the vibration of stator. The tilted side of the slider was shaped with a "[" like groove in order to match the bottom connection part of the torsion spring. The tilted angle β was supplementary to the α angle of the spring in order that the upper base would be perpendicular to the wall of the bracket. In this arrangement, the stator would contact with the rotors when the slider moved up and the pre-pressure at the contact faces would be applied and modulated through the deformation of the torsion spring [26].

The pre-pressure between rotor and stator could be adjusted by deforming the torsion spring, which could be evaluated by the value of α angle. In particular, by changing the α angle, namely the deformation of the torsional spring, the pressure between the driving feet and the outside surface of the driving disks could be adjusted. In order to keep the included angle θ always at 180°, the tilted angle β should be changed accordingly. Experimental results illustrated that 57° α angle represents the best deformation for applying a suitable preload on contact faces, thus 123° was selected for defining β of the supporting slider.
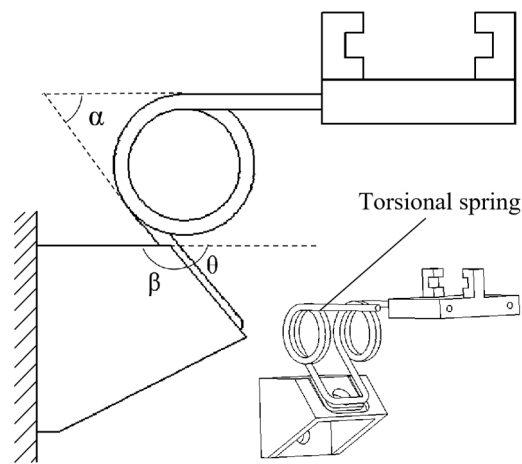
Figure 3. Structure of pre-pressure modulating unit.

3. Operating Principle Analysis

The working principle of the dual-rotor ultrasonic motor is shown in Figure 4. When applying single-phased sinusoidal signal with resonant frequency to piezoelectric ceramic wafer, it excited the ultrasound vibration of the stator due to the inversed piezoelectric effect. The vibration of the driving feet at two ends of the fixed metal plate drove the driving disks pressed on it to rotate by the contact friction, thereby enabling the parallel shafts to rotate in a reversed direction at the same time. The vibration mode for the ultrasonic motor was the first longitudinal in-plane vibration mode. The vibration direction of the driving foot at each end was opposite to each other [27,28]. The longitudinal vibration of the metal plate caused the driving foot to have a linear motion along the surface of the shaft and to push the shaft to rotate in one direction. Due to the central symmetry of the structural design and the engagement of the gear unit, rotary directions for the two rotors were opposite, that is, the left rotor rotated clockwise, the right rotor rotated counterclockwise.
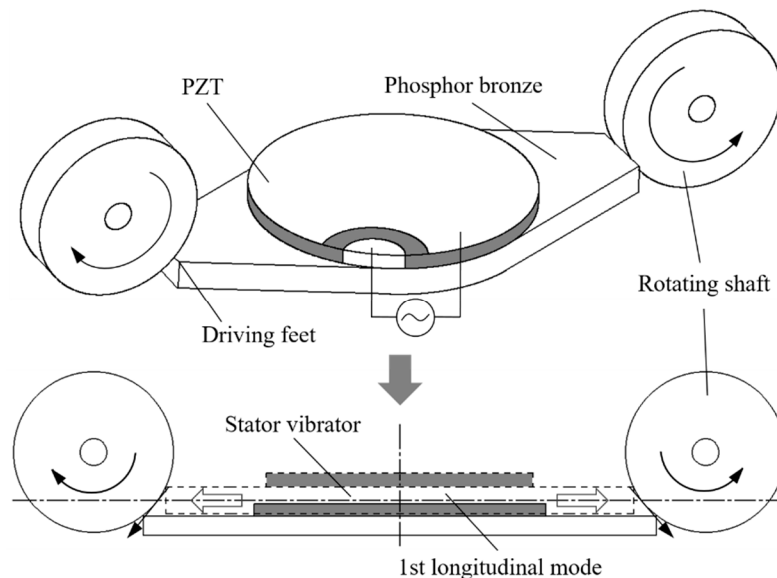
Figure 4. Operating principles of dual-rotor ultrasonic motor.

The appearance size of the spindle-shaped stator was 20 mm × 35 mm × 2 mm (width × length × thickness), and the driving feet at both ends was 5 mm in width. The piezoelectric wafer was Ø20 mm × 1 mm and polarized in the thickness direction. The ground electrode at the bottom face of the wafer was extended from the side to the top face for connection. The rotating shaft was 12 mm

in diameter and 3 mm in thickness, and the distance between the two parallel shafts was 43 mm. The stator was assembled to the bottom-center position between the rotating shafts with its dual driving feet contacting both shafts. In order to determine the stator's vibration mode and frequency, the finite element method-based simulation software COMSOL Multiphysics was utilized to perform the eigenfrequency analysis. Sequentially, frequency domain analysis was performed to obtain the vibration displacement at resonance. During the simulation, all material properties were assumed to be constant, which means the non-linear effect of materials (e.g., hysteresis of piezoelectric material) was not taken into consideration. Phosphor bronze and PZT-8H were selected for the metal plate and piezoelectric wafer, respectively. In particular, PZT-8H material has a piezoelectric constant d_{33} of 200×10^{-12} C/N, electromechanical coupling factor k_{33} of 0.60, mechanical quality factor Q_{m} of 800, dielectric dissipation factor $\tan\delta$ of 0.5%, density of 7450 kg/m^3, and Curie temperature T_{c} of 300 °C [29,30]. For this numerical simulation, the three-dimensional model of the stator was meshed into 8385 free tetrahedral elements and all physical boundaries of the stator were set to be free.

Calculation results from the eigenfrequency analysis are plotted in Figure 5a. It was observed that the metal plate vibrated in the first longitudinal mode, which demonstrated the working principle of the stator. The resonance frequency of this working mode was 61.4 kHz. With the voltage of 150 V (peak-to-peak) at resonance, the calculated results from the frequency domain analysis reveal that the first longitudinal vibration amplitude of the stator was about 1.4 microns. When the stator extended, the driving foot pushed driving disks to rotate shafts from the initial position (top figure) to the new position (left figure). After that, the stator returned to the original state (bottom figure) and the contact friction between the stator and rotors decreased, leading to the continuous rotation of rotors. Sequentially, the stator kept contracting (right figure), but the rotor still kept rotating in the same direction with the assistance of inertia. Generally, these deformation cycles for stator were repeated periodically to investigate the revolutions of both rotors. The transient vibration response of the stator was simulated and the vibration amplitude of the driving foot when the applied AC voltage was 150 V$_{\mathrm{p-p}}$ is plotted in Figure 5b.
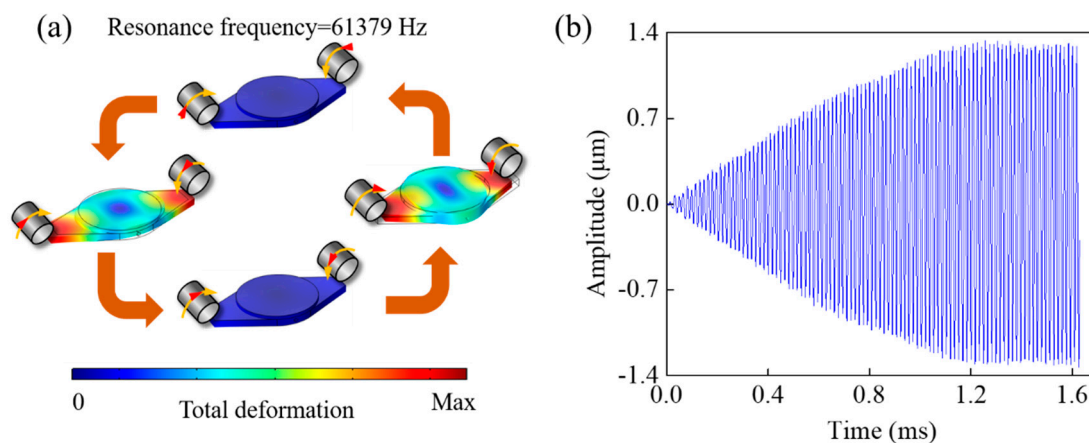
Figure 5. Simulated vibration of the stator. (**a**) Vibration mode, and (**b**) transient response.

4. Experimental Results and Discussions

According to the structure and size parameters mentioned above, a prototype dual-rotor ultrasonic motor was fabricated (see Figure 6). A laser Doppler vibrometer system (PSV-500-3D) was used to measure the vibration characteristics of the stator. Figure 7 depicts the measured average vibration magnitude versus operating frequency when the stator unit was driven by 150 V (peak-to-peak) voltage. It can be seen that the resonance frequency was 62.56 kHz, which was 1.18 kHz higher than the simulation value (61.38 kHz), and may have been caused by the deviation in the fabrication and assembling processes. In addition, the pressure forces and the twisting loads which were neglected during the simulation also contributed to the discrepancy between the calculated and measured

frequencies. The vibration pattern shown in the inset agreed well with the calculated working mode shown in Figure 5. With the excitation voltage of 150 V_{p-p} at resonance, the measured amplitude was 1.5 microns. The measured vibration displacements with 300 V_{p-p} and 50 V_{p-p} were 2.8 and 0.4 microns, respectively.
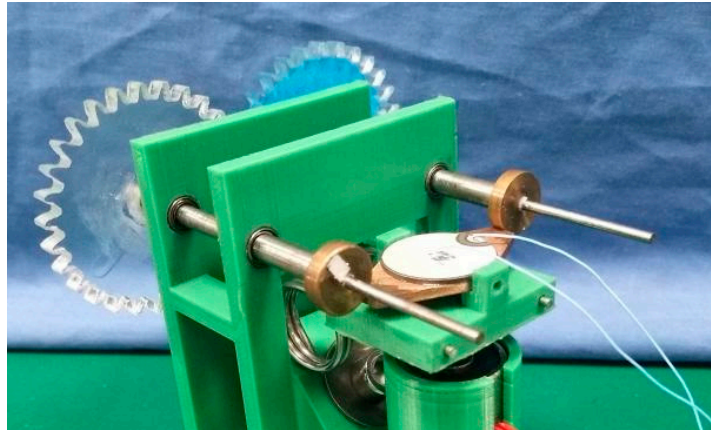

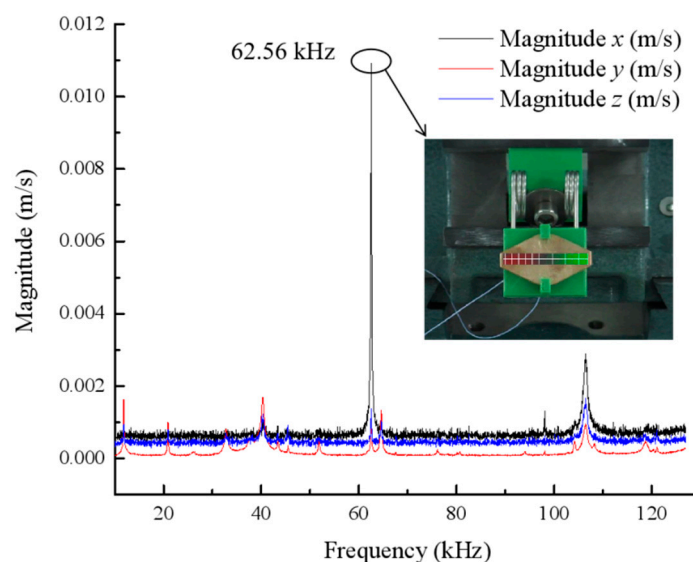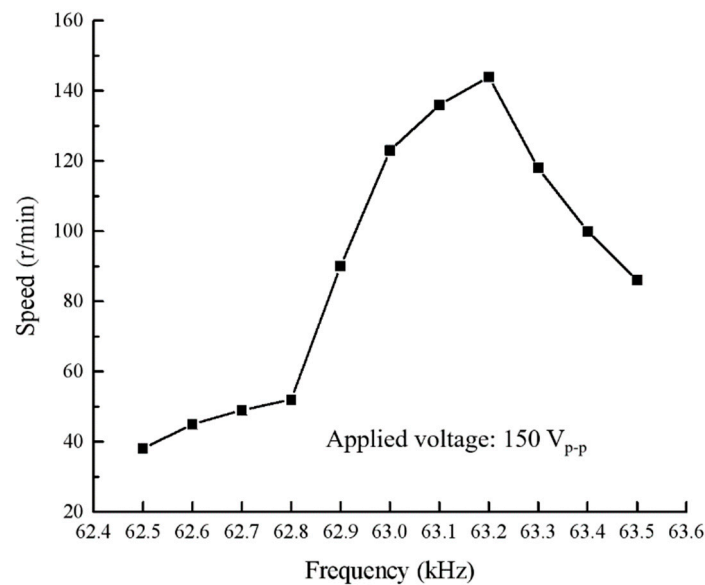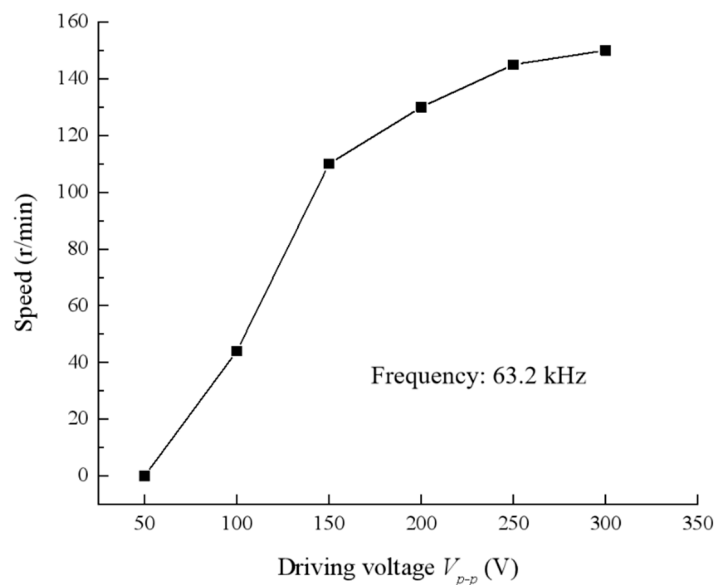**Figure 6.** Image of the prototype motor.

Figure 7. Vibration measurement of the stator.

In order to measure the speed of the motor, a reflective marker was attached to the rotor and the measurement was carried out by a non-contact laser velocimeter (DT-2234B). In the following experiments, unless otherwise specified, the prototype motor was applied with the driving voltage of 150 V_{p-p} and operated at resonance. The relationship between the no-load speed and the driving frequency with the excitation voltage maintained at 150V_{p-p} is plotted in Figure 8. It was observed that the maximum speed of the motor could reach 144 r/min with the driving frequency of 63.2 kHz. The lower output speed at other driving frequencies indicated that the working behavior of the prototype motor was very sensitive to the operating frequency. Besides, effects of applied voltage at the same operating frequency were measured and results are displayed in Figure 9. It can be seen that with the same driving frequency, the speed of the prototype motor increased as the input voltage was increased. This was because when the motor worked near the resonance frequency, its output speed was determined by the stator's vibration amplitude. It should also be noticed that the increase of the rotating speed appeared non-linearly and reached a maximum value of 150 r/min when the applied

voltage increased to 300 V_{p-p}, indicating the increase of driving voltage could improve the output performance to a limited extent.

Figure 8. No-load rotating speed versus the driving frequency.

Figure 9. No-load rotating speed versus the driving voltage.

In addition, the dependence of the pre-pressure upon the rotating speed of the prototype motor was investigated by dynamic pre-pressure adjustment with an electromagnet modulator [31]. It was mainly composed of a permanent magnet (Ø10 mm × 5 mm), a guiding cylinder, an electromagnet (Ø20 mm × 15 mm), and a bolt. The permanent magnet was fixed to the bottom face of the base and the electromagnet was fixed to the bracket with a 3 mm gap to the permanent magnet. By adjusting the DC voltage applied to the electromagnet, the changed magnetic force was capable of modulating the pre-pressure between stator and rotor. Figure 10 shows the measured no-load speed versus the pre-pressure. It can be seen that the rotating speed increased from 47 r/min to 57 r/min with the pre-pressure decreasing from 3.25 N to 1.95 N. Dynamic pre-pressure modulation could be used as a rough adjustment strategy when the prototype motor is installed to the underwater robot and the manual positioning of the pre-pressure modulation unit becomes inconvenient.
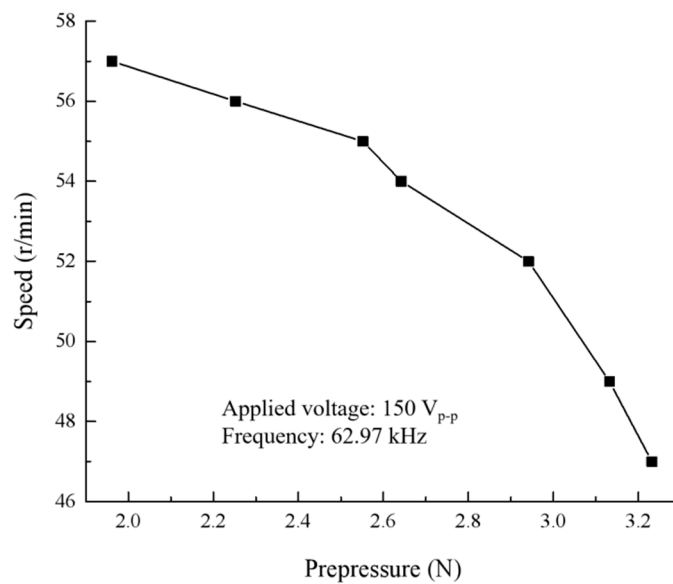
Figure 10. Relationship between the no-load rotating speed and the pre-pressure.

The mechanical characteristics of the prototype motor were measured and results are shown in Figure 11. It can be seen that the stalling torque was 3 mN·m, the no-load speed was 110 r/min, and the maximum output power was about 7.5 mW corresponding to the output torque of 1.2 mN·m and rotating speed of 60 r/min. Both rotors were tested respectively and there were no obvious differences in mechanical characteristics between the two rotors. Compared to our previous inertial-type ultrasonic motors designed for actuating underwater robots [24], the output torque for individual rotor increased 2.4 times. Measured results show that the prototype motor had a good performance at a driving frequency of around 63.2 kHz.
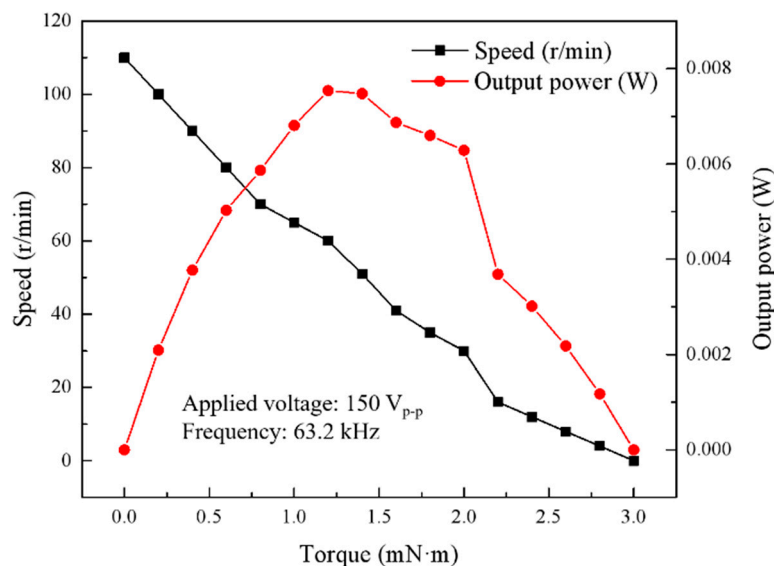

**Figure 11.** Mechanical characteristics of the prototype motor.

Finally, we fabricated a cylindrical underwater robot model according to the conceptual design shown in Figure 1 to test the propulsion behavior of the prototype motor. The prototype motor was installed to the end part of the robot model and one pair of thrusters with reversed turning directions were respectively mounted to each rotating shaft end of the motor. Counter weights were placed at the bottom face of the robot model's middle part for balancing the attitude during propulsion.

The appearance size of the robot model was Ø80 mm × 210 mm and the mass was 295 g. The underwater propulsion experiment was conducted and the propelling process was captured, as shown in Figure 12. It was observed that the immersed robot model, propelled by the dual-rotor ultrasonic motor, moved smoothly from the right side to the left side with the displacement of 520 mm in 20 s. Variance of the propulsion velocity was measured and plotted as the black points shown in Figure 13. For comparison, simulated results based on the methods in our prior study [24] were also plotted as the red line shown in Figure 13. The inset shows the ambient flow distribution around the robot model. It was observed from the tested results that the underwater robot experienced an accelerating state in the first 6 s, then moved at a relatively steady velocity of 30 mm/s for 9 s, and then decelerated gradually to 25 mm/s for the last 3 s. Simulated results showed a faster acceleration process (~4 s) and higher steady state velocity (~36 mm/s), which may have been caused by the simplification of the robot model geometry. In addition, hysteresis effects of piezoelectric materials not considered during the simulation may have also suppressed the propulsion velocity when the robot model operated for a long time. Nonetheless, experimental results basically agreed with the calculated propulsion process, proving that the proposed dual-rotor ultrasonic motor could effectively actuate the underwater robot model.
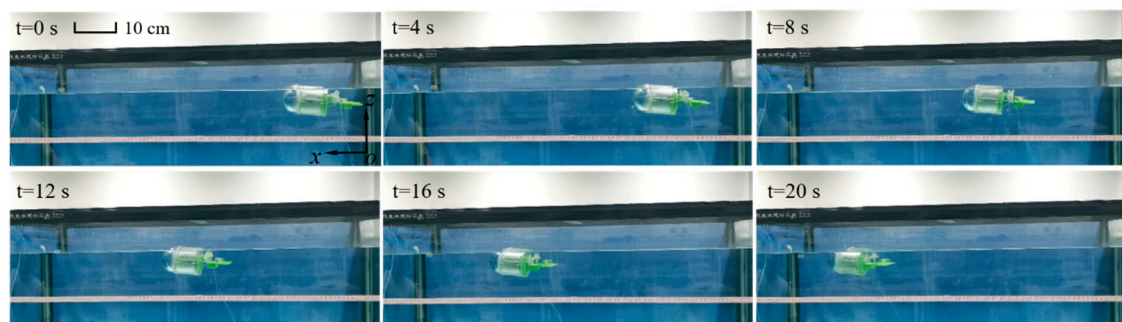
Figure 12. Captured forward propelling process of the underwater robot model.
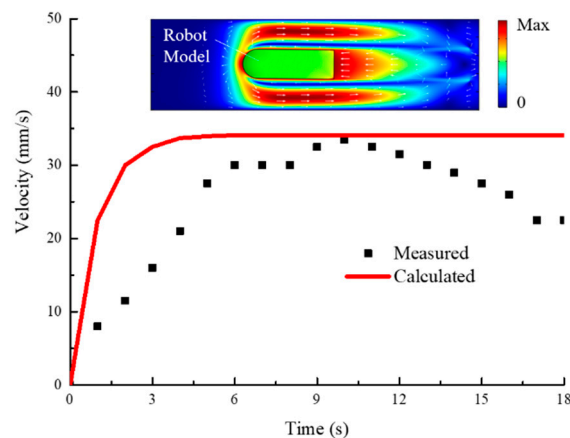
Figure 13. Propulsion velocity variation versus propelling time.

5. Conclusions

In this work, a novel dual-rotor ultrasonic motor for underwater propulsion was presented and studied. Because of the features of dual output shafts and its compact structure, the proposed ultrasonic motor can provide effective propulsion and meet the requirements of miniaturization for MUVs. With the finite element simulation, the size and working mode of the stator were determined. A prototype motor was fabricated and the measured vibration characteristics of the stator confirmed the proposed working principle. The no-load speed for the prototype motor was about 110 r/min and the stalling torque was around 3.0 mN·m. Equipped with the prototype motor, one 295 g cylindrical underwater robot model could move at 33 mm/s. With the common non-magnetic-interference feature

of piezoelectric actuators, the proposed ultrasonic motor with dual rotating shafts is promising for propelling MUVs to perform specific underwater explorations, such as geomagnetic field detection, etc.

References

1. Bogue, R. Underwater robots: A review of technologies and applications. *Ind. Robot* **2015**, *42*, 186–191. [CrossRef]
2. Shi, L.; Guo, S.; Asaka, K. Development of a novel underwater microrobot with proximity sensors. In Proceedings of the 2011 IEEEIICME International Conference on Complex Medical Engineering, Harbin, China, 22–25 May 2011; pp. 69–73.
3. Ambar, R.B.; Sagara, S.; Yamaguchi, T. Development of a dual-shaft propeller thruster equipped with rotational speed sensor for UVMS control. In Proceedings of the Eighteenth International Symposium on Artificial Life and Robotics 2013, Daejeon, Korea, 30 January–1 February 2013; pp. 241–247.
4. Li, X.; Chen, D.; Jin, J.; Wang, L. A novel underwater piezoelectric thruster with one single resonance mode. *Rev. Sci. Instrum.* **2019**, *90*, 045007. [CrossRef] [PubMed]
5. Nguyen, Q.S.; Heo, S.; Park, H.C.; Byun, D. Performance evaluation of an improved fish robot actuated by piezoceramic actuators. *Smart Mater. Struct.* **2010**, *19*, 035030. [CrossRef]
6. Nguyen, Q.S.; Heo, S.; Park, H.C.; Goo, N.S.; Kang, T.; Yoon, K.J.; Lee, S.S. A fish robot driven by piezoceramic actuators and a miniaturized power supply. *Int. J. Control Autom.* **2009**, *7*, 267–272. [CrossRef]
7. Ku, K.; Bradbeer, R.S.; Lam, K.; Yeung, L.F.; Li, R. A Novel Actuator for Underwater Robots. *IEEE J. Ocean. Eng.* **2009**, *34*, 331–342. [CrossRef]
8. Wiguna, T.; Park, H.C.; Heo, S.; Goo, N.S. Experimental parametric study of a biomimetic fish robot actuated by piezoelectric actuators. In Proceedings of the Active and Passive Smart Structures and Integrated Systems, San Diego, CA, USA, 27 April 2007; p. 65250R.
9. Hu, Z.; Yang, Y.; Lin, Y. Failure analysis for the mechanical system of Autonomous Underwater Vehicles. In Proceedings of the 2013 International Conference on Quality, Reliability, Risk, Maintenance, and Safety Engineering, Sichuan, China, 15–18 July 2013; pp. 943–948.
10. Showalter, S. The Legal Status of Autonomous Underwater Vehicles. *Mar. Technol. Soc. J.* **2004**, *38*, 80–83. [CrossRef]
11. Watson, S.A.; Green, P.N. Design considerations for Micro-Autonomous Underwater Vehicles (μAUVs). In Proceedings of the 2010 IEEE Conference on Robotics, Automation and Mechatronics, Singapore, 28–30 June 2010; pp. 429–434.
12. Meng, L.; Lin, Y.; Gu, H.; Xu, H.; Geng, L. A new type of small underwater robot for small scale ocean observation. In Proceedings of the 6th Annual IEEE International Conference on Cyber Technology in Automation, Control and Intelligent Systems, Chengdu, China, 19–22 June 2016; pp. 152–156.
13. Uchino, K. Piezoelectric ultrasonic motors: Overview. *Smart Mater. Struct.* **1998**, *7*, 273–285. [CrossRef]
14. Wen, J.; Wan, N.; Wang, R.; Chen, S.; Zheng, J.; Li, J. A Novel Linear Walking Type Piezoelectric Actuator Based on the Parasitic Motion of Flexure Mechanisms. *IEEE Access* **2019**, *7*, 25908–25914. [CrossRef]
15. Wan, N.; Wen, J.; Hu, Y.; Kan, J.; Li, J. A parasitic type piezoelectric actuator with an asymmetrical flexure hinge mechanism. *Microsyst. Technol.* **2019**, 1–8. [CrossRef]
16. Zhao, C. *Ultrasonic Motors: Technologies and Applications*; Springer Science & Business Media: Berlin, Germany, 2011.

17. Wang, L.; Lu, X.; Zhao, C.; Xue, C. A novel high-speed rotary ultrasonic motor applied to micro air vehicles. In Proceedings of the 2016 Symposium on Piezoelectricity, Acoustic Waves, and Device Applications (SPAWDA), Xi'an, China, 21–24 October 2016; pp. 186–188.

18. Wang, L.; Wang, Y.; Lu, X.; Zhao, C. A new type of rotary ultrasonic motor applied to micro air vehicles. *J. Vib. Meas. Diagn.* **2018**, *38*, 170–175.

19. Wang, L.; Wang, Y.; Lu, X.; Zhao, C. Note: A disk-shaft shaped high-speed rotary ultrasonic motor. *Rev. Sci. Instrum.* **2018**, *89*, 126106. [CrossRef] [PubMed]

20. Hunstig, M. Piezoelectric Inertia Motors—A Critical Review of History, Concepts, Design, Applications, and Perspectives. *Actuators* **2017**, *6*, 7. [CrossRef]

21. Liu, Y.; Wang, Y.; Liu, J.; Xu, D.; Li, K.; Shan, X.; Deng, J. A Four-Feet Walking-Type Rotary Piezoelectric Actuator with Minute Step Motion. *Sensors* **2018**, *18*, 1471. [CrossRef] [PubMed]

22. Liu, Y.; Chen, W.; Shi, D.; Tian, X.; Shi, S.; Xu, D. Development of a Four-Feet Driving Type Linear Piezoelectric Actuator Using Bolt-Clamped Transducers. *IEEE Access* **2017**, *5*, 27162–27171. [CrossRef]

23. Liu, J.; Liu, Y.; Zhao, L.; Xu, D.; Chen, W.; Deng, J. Design and Experiments of a Single-Foot Linear Piezoelectric Actuator Operated in a Stepping Mode. *IEEE Trans. Ind. Electron.* **2018**, *65*, 8063–8071. [CrossRef]

24. Wang, L.; Hou, Y.; Zhao, K.; Shen, H.; Wang, Z.; Zhao, C.; Lu, X. A novel piezoelectric inertial rotary motor for actuating micro underwater vehicles. *Sens. Actuat. A Phys.* **2019**, *295*, 428–438. [CrossRef]

25. Čeponis, A.; Mažeika, D. An inertial piezoelectric plate type rotary motor. *Sens. Actuat. A Phys.* **2017**, *263*, 131–139. [CrossRef]

26. Luo, X.; Xu, J.; Luo, Q.; Wang, R. Design and research on support plate torsion spring of special electromechanical device. In Proceedings of the IEEE 2011 Second International Conference on Mechanic Automation and Control Engineering, Inner Mongolia, China, 15–17 July 2011; pp. 1162–1164.

27. Aoyagi, M.; Suzuki, F.; Tomikawa, Y.; Kano, I. High-Speed Thin Ultrasonic Spindle Motor and Its Application. *Jpn. J. Appl. Phys.* **2004**, *43*, 2873–2878. [CrossRef]

28. Chen, W.; Liu, Y.; Liu, J.; Shi, S. A Linear Ultrasonic Motor Using Bending Vibration Transducer with Double Driving Feet. *Ferroelectrics* **2010**, *400*, 221–230. [CrossRef]

29. Lu, X.; Hu, J.; Yang, L.; Zhao, C. A novel in-plane mode rotary ultrasonic motor. *Chin. J. Aeronaut.* **2014**, *27*, 420–424. [CrossRef]

30. Lu, X.; Hu, J.; Yang, L.; Zhao, C. A novel dual stator-ring rotary ultrasonic motor. *Sens. Actuat. A Phys.* **2013**, *189*, 504–511. [CrossRef]

31. Shi, S.; Xiong, H.; Liu, Y.; Chen, W.; Liu, J. A ring-type multi-DOF ultrasonic motor with four feet driving consistently. *Ultrasonics* **2017**, *76*, 234–244. [CrossRef] [PubMed]